

Investigating the Photostability of Organic Photovoltaics for Indoor and Outdoor Applications

Andrew J. Clarke, Emily J. Yang, Suzanne K. Thomas, Harrison K. H. Lee, Ann Hunter, Weixia Lan, Matthew J. Carnie, Ji-Seon Kim, and Wing Chung Tsoi*

Organic photovoltaics (OPVs) show great promise for both outdoor and indoor applications. However, there remains a lack of understanding around the stability of OPVs, particularly for indoor applications. In this work, the photostability of the poly[(thiophene)-alt-(6,7-difluoro-2-(2-hexyloxy)quinoxaline)]_{2,2'}-((2Z,2'Z)-((4,4,9,9-tetrahexyl-4,9-dihydro-s-indaceno[1,2-b:5,6-b']dithiophene-2,7-diyl)bis(methanylylidene))bis(3-oxo-2,3-dihydro-1H-indene-2,1-diylidene)) dimalononitrile blend is investigated for both outdoor and indoor applications. Photostability is found to vary drastically with illumination intensity. Devices under high-intensity white light-emitting diode (LED) illumination, with their short-circuit current density (J_{SC}) matching J_{SC-EQE} for AM1.5 G illumination, lose 42% of their initial performance after 30 days of illumination. Contrastingly, after almost 47 days of illumination devices under 1000 lux white LED illumination show no loss in performance. The poor photostability under 1 sun illumination is linked to the poor photostability of IDIC. Through Raman spectroscopy and mass spectrometry, IDIC is found to suffer from photoisomerization, which detrimentally impacts light absorption and carrier extraction. In this work, it is highlighted that under low light levels, the requirement of intrinsic material photostability may be less stringent.

photovoltaic performances of over 31% have been achieved, exceeding those obtained for silicon photovoltaics.^[2,3] Using OPVs for indoor light harvesting has the potential to provide power for a range of low power electronics, such as sensors, and data transmitters as part of the internet of things. Compared to the solar spectrum, the emission spectra of indoor light sources tend to be located in the visible region of the light spectrum (around 390–760 nm). This overlaps well with the absorption spectra of many organic semiconductors used for OPV applications.


One of the major concerns with OPVs is their stability, with photostability being one area of concern. This has been investigated extensively for 1 sun applications.^[4] There have been several demonstrations of outstanding stability with extrapolated lifetimes exceeding 10 years in some cases.^[5–7] However, this behavior is strongly dependent on the choice of photoactive materials, and in many cases poor photostability and device lifetimes are observed. A range of

1. Introduction

Through continued innovation in material design and device engineering, rapid performance improvements have been achieved for organic photovoltaics (OPVs) over the past 20 years. Outdoor performances of over 18% have now been demonstrated for binary OPVs for 1 sun applications, approaching that of silicon photovoltaics.^[1] The interest in OPVs for indoor applications has also attracted significant interest in recent years, where

reasons have been identified behind the varying photostability of OPVs, including the photo-dimerization of fullerenes,^[8–10] the photoinduced fragmentation of molecular materials,^[11] photoinduced chemical or structural changes,^[5,11–16] and morphological changes.^[5,17–20] Studies have also investigated degradation as a function of higher light intensities to consider accelerated aging.^[21] However, there has been much less focus on the stability of OPVs for indoor applications. This area is interesting as stresses are likely to be lower with reduced light

A. J. Clarke, S. K. Thomas, H. K. H. Lee, M. J. Carnie, W. C. Tsoi
SPECIFIC
Swansea University
Swansea SA1 8EN, UK
E-mail: W.C.Tsoi@swansea.ac.uk

 The ORCID identification number(s) for the author(s) of this article can be found under <https://doi.org/10.1002/aesr.202300285>.

© 2024 The Authors. Advanced Energy and Sustainability Research published by Wiley-VCH GmbH. This is an open access article under the terms of the Creative Commons Attribution License, which permits use, distribution and reproduction in any medium, provided the original work is properly cited.

DOI: 10.1002/aesr.202300285

E. J. Yang, J.-S. Kim
Department of Physics
Imperial College London
London SW7 2AZ, UK

A. Hunter
NMSF
Swansea University
Swansea SA2 8PP, UK

W. Lan
School of Mechatronic Engineering and Automation
Shanghai University
Shanghai 200444, P. R. China

intensities and reduced temperatures and also potentially reduced lifetime requirements, which could mean that the required lifetimes are much easier to achieve for indoor applications.

In this work the photostability of poly[(thiophene)-alt-(6,7-difluoro-2-(2-hexyldecyloxy)quinoxaline)] (PTQ10):2,2'-((2Z,2'Z)-((4,4,9,9-tetrahexyl-4,9-dihydro-s-indaceno[1,2-b:5,6-b'] dithiophene-2,7-diyl)bis(methanylylidene))bis(3-oxo-2,3-dihydro-1H-indene-2,1-diylidene))dimalononitrile (IDIC) devices are investigated under white light-emitting diode (LED) illumination for outdoor and indoor applications. Drastically different stability behavior is observed. A strong burn-in and continued longer-term degradation is observed during high-intensity illumination resulting in a 42% drop in PCE over 30 days of illumination. Contrastingly, no obvious deterioration in performance is observed over almost 47 days of continuous 1000 lux illumination. For devices aged under 1 sun equivalent intensity illumination, increased carrier trapping is observed alongside a continuous reduction in external quantum efficiency (EQE) with increasing illumination time. Through investigating the photostability of PTQ10 and IDIC, it is found that IDIC has poor photostability, resulting in photobleaching and a widening of the bandgap. The photodegradation product of IDIC is found to be mass-invariant, and Raman spectroscopy is used to identify an isomeric degradation product.

2. Results and Discussion

PTQ10 was reported to have a simple, high yield synthesis, and promising performance, which are ideal properties for

large-area, upscaled manufacturing.^[22] In addition to this, the absorption spectrum of PTQ10 overlaps well with the emission spectra of common indoor light sources (**Figure 1**). Combined with its potential low cost, which is particularly important for indoor applications where the generated power is very low, this makes PTQ10 an interesting candidate material for indoor applications. PTQ10 was blended with IDIC in this work, due to promising initial reports for the performance of this blend for outdoor applications.^[22] Inverted devices were fabricated and device efficiencies of 10.6% and 18.5% were obtained under 1 sun AM1.5 G and 1000 lux 4000 K white LED illumination (Table S1 and Figure S1, Supporting Information).

The photostability of these devices was monitored under white LED illumination (**Figure 2**). The encapsulated devices were located in a nitrogen-purged chamber for the duration of stability measurements to eliminate the potential for photooxidation.

For all stability measurements, the short-circuit current density (J_{SC}) was matched to J_{SC-EQE} values (Table S1, Supporting Information) calculated from EQE spectra (Figure S1c,d, Supporting Information) for 1 sun AM1.5 G or 1000 lux 4000 K white LED illumination, by adjusting the light intensity. The emission spectra of the white LEDs used for performance characterization and photostability studies are shown in Figure S2, Supporting Information. The light source used for stability measurements contains no UV, NIR, or IR irradiation. The fluctuations in the photovoltaic parameters at 1000 lux are due to slight instabilities in the light intensity at low-supplied currents to the LED array, with the fluctuations occurring on a 24 h cycle, possibly due to fluctuating temperatures within the laboratory on a daily cycle. The gap in the indoor data

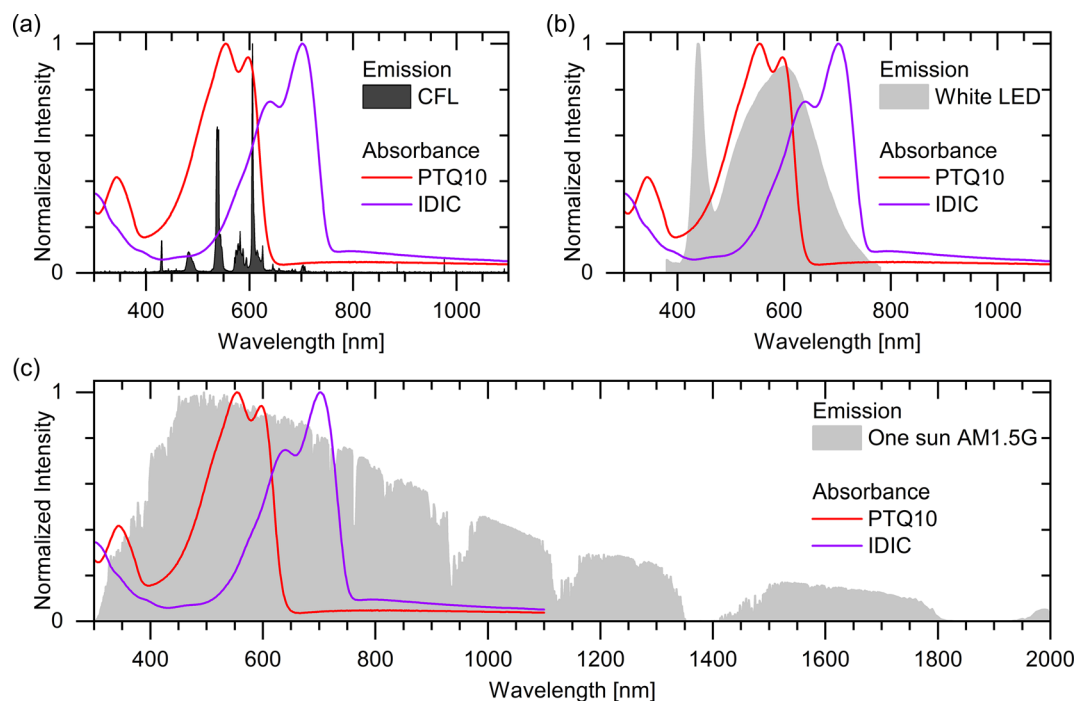


Figure 1. UV–visible absorption spectra of PTQ10 and IDIC shown alongside the typical emission spectra of a) compact fluorescent lamps, b) white LEDs, and c) 1 sun AM1.5 G illumination.

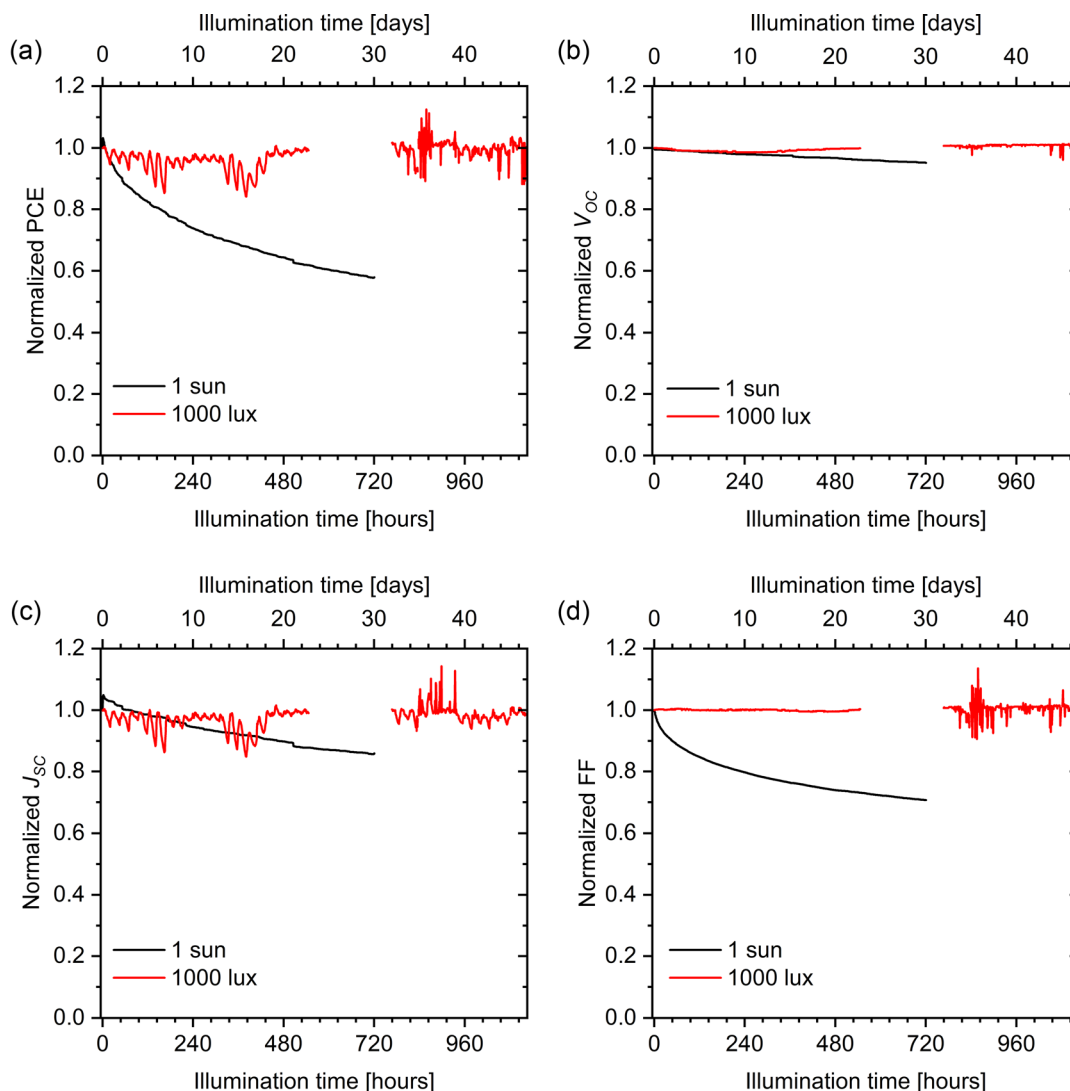


Figure 2. Photovoltaic parameters of PTQ10:IDIC devices measured during photostability measurements under white LED illumination at different light intensities.

between ≈ 500 and 720 h is due to the data logging software crashing during this period; however, illumination was continuous throughout.

During 1 sun equivalent intensity illumination, there is a rapid burn-in, with a continued longer-term more gradual deterioration in performance. All photovoltaic parameters are affected, but the J_{sc} and fill factor are impacted most strongly, resulting in a loss of $\approx 42\%$ of the initial device performance after 30 days of continuous illumination. In contrast, under 1000 lux illumination, there is no obvious deterioration in any of the photovoltaic parameters over almost 47 days of continuous illumination.

Transient photovoltage (TPV) and transient photocurrent (TPC) measurements were performed on PTQ10:IDIC devices aged under the two different illumination conditions to understand how the carrier behavior was impacted by photoaging (Figure 3). No change in carrier density was observed after 7 days of continuous 1000 lux white LED illumination, measured as a

function of V_{oc} . In contrast, for the device aged under 1 sun equivalent intensity illumination, after 7 days of photoaging there was approximately a 40% increase in the carrier density. Such an increase in carrier density required to achieve the same V_{oc} is indicative of an increased density of trap states.^[14,23–27] TPV measurements showed no change in the lifetime of laser-pulse-generated carriers with 7 days of 1000 lux illumination. However, for devices aged for 7 days under 1 sun equivalent intensity white LED illumination, the carrier lifetime increases. This change suggests that the additional trap states are most likely shallow traps, from which trapped carriers can become thermally detrapped, thereby increasing their lifetime.^[14,25,28] These differences in carrier behavior under different light levels are consistent with the observed differences in device photostability.

To better understand what may be causing the photoinduced deterioration in performance and increased carrier trapping

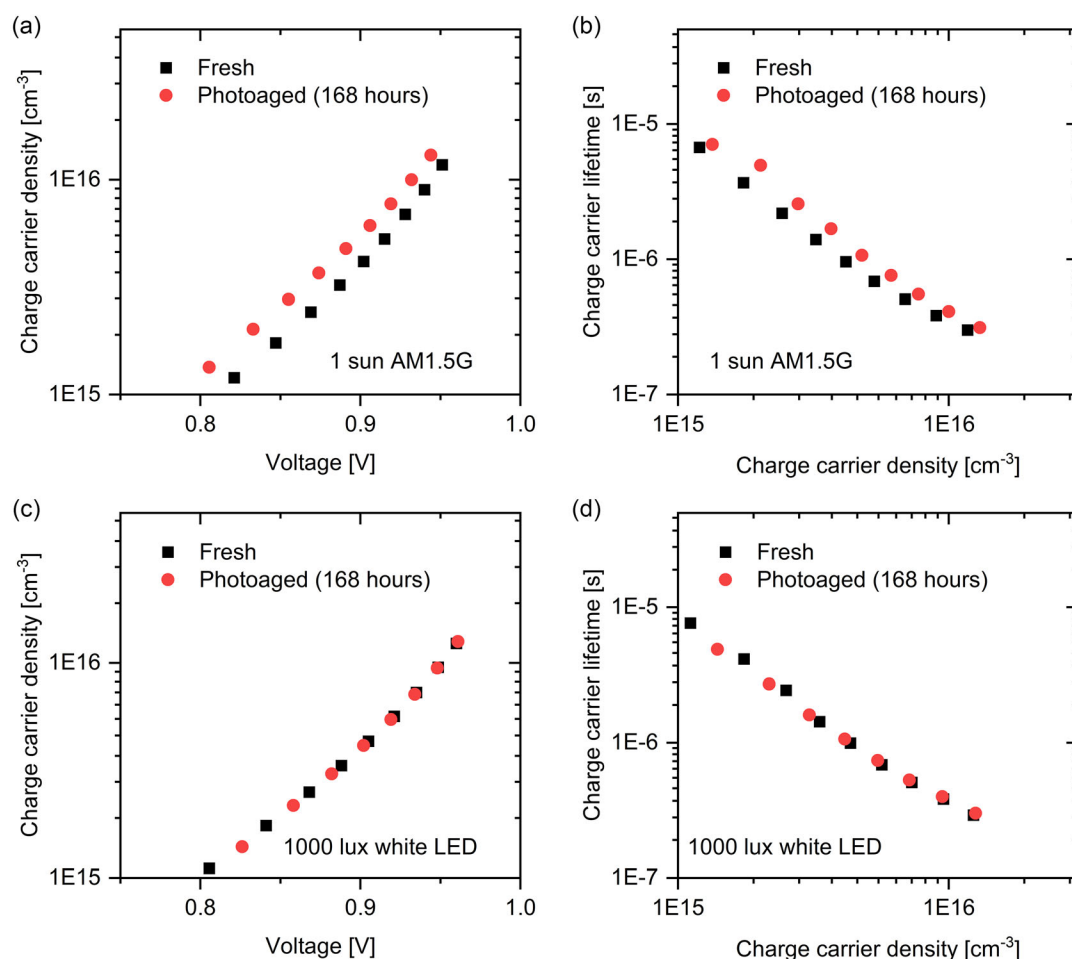


Figure 3. Transient optoelectronic characterization of PTQ10:IDIC devices. Devices aged under a,b) 1 sun equivalent white LED and c,d) 1000 lux white LED illumination. a,c) TPC measurements to determine the carrier density as a function of V_{OC} . b,d) TPV measurements to determine lifetime of laser-pulse-generated carriers as a function of carrier density, measured under open-circuit conditions.

with high-intensity illumination, further characterization was performed. UV-visible spectra of PTQ10:IDIC blend films, and neat PTQ10 and IDIC films were measured during 1 sun equivalent intensity white LED illumination (Figure 4). No changes are observed to the PTQ10 absorption spectrum as a result of continuous illumination, suggesting that PTQ10 is relatively photostable. However, IDIC suffers from strong photobleaching, with a 55% decrease in the absorbance of the 0–0 absorption peak after 336 h of illumination. There is also an increase in absorption between 420 and 560 nm, with the formation of a new high-energy shoulder at around 550 nm, which may also account for the increase in the relative intensity of the 0–1 to 0–0 absorption peaks with increased photoaging time. An overall blueshift of the IDIC absorption is also observed. These changes to IDIC are indicative of photodegradation, with a bleaching of the chromophores and increase in high-energy absorption indicative of disruption to the molecular conjugation. This behavior is remarkably similar to what has been observed previously for ITIC.^[14,29]

In the blend, photodegradation is also observed, albeit at a much slower rate. There is a 3.5% decrease in the 0–0 absorption

peak after 336 h of illumination. Reduced photobleaching in the blend could be explained from comparatively less light being absorbed by the IDIC due to the presence of the polymer, and increased quenching of the excited state within the blend, which can inhibit excited state mediated degradation reactions. Such behavior has been reported previously for a range of donor–acceptor blends.^[13,14,30,31]

EQE spectra were also measured during photoaging (Figure S3, Supporting Information). Interestingly, while the losses in absorption in the PTQ10:IDIC blend as a result of photobleaching are predominantly in the region from 575 to 750 nm, where IDIC absorption dominates, there are decreases in EQE across the whole spectrum. For example, between 450 and 600 nm, where PTQ10 absorption dominates, there is still a clear decrease in the EQE despite the absorption of PTQ10 being stable. This suggests that it is not only the decrease in absorption that is contributing toward to the decrease in performance with increasing illumination time. Rather, it indicates that there are also additional inefficiencies in charge separation, transport, and/or collection, which is consistent with the observed increase in trap density.

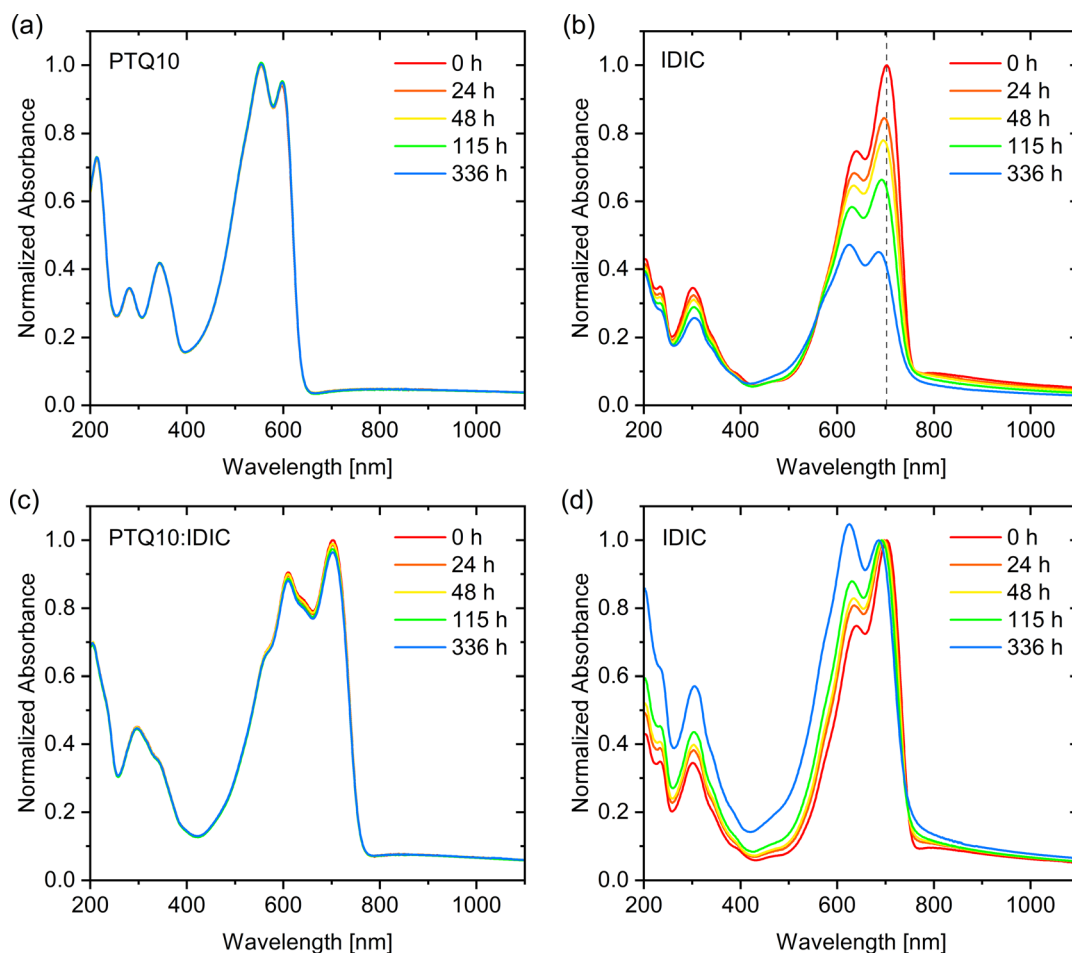


Figure 4. UV-visible spectra of a) PTQ10, b,d) IDIC, and c) PTQ10:IDIC during photoaging under 1 sun equivalent white LED illumination. Spectra in (a–c) are normalized by dividing the whole spectrum by the intensity of the most intense peak in the 0 h spectra. Spectra in (d) are normalized to the 0–0 absorption peak to illustrate the blueshift.

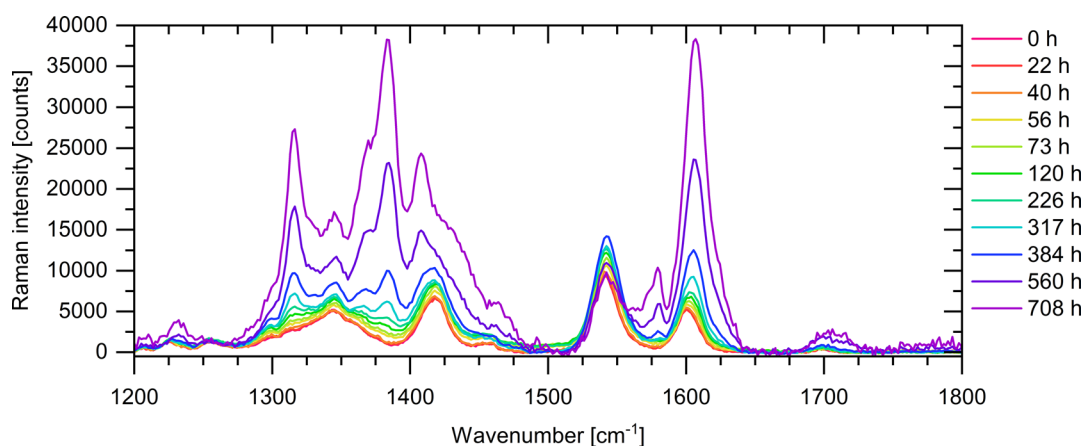


Figure 5. Raman spectra of IDIC measured with increased photoaging time under 1 sun white LED illumination.

To study the origins of the observed IDIC photobleaching, Raman spectra of IDIC films were measured with increasing photoaging time (Figure 5). The overall intensity of the

Raman spectrum increases with increasing aging time, which can be attributed to the increased Raman resonance with the increase in absorption at the 532 nm excitation wavelength

during photoaging (Figure 4b). There are also significant changes to the peaks in the Raman spectra. To highlight a few, there is a significant increase in the Raman intensity at 1375 and 1600 cm^{-1} as well as a new peak at 1580 cm^{-1} .

The Raman spectrum of the blend shows no obvious changes after 708 h of white LED illumination (Figure S4a, Supporting Information). However, the blend spectrum is dominated by peaks associated with PTQ10. Additionally, given that the UV-visible spectroscopy demonstrates that the rate of photodegradation in the blend is significantly slower than for the neat film, it may be that the photodegradation is too small to be observed clearly in the blend. To probe the blend further, in situ measurements were performed using the Raman laser to simulate accelerated aging (Figure S4b–d, Supporting Information). The intensity of the Raman laser spot during these measurements was calculated to be $\approx 1.8 \times 10^6 \text{ W m}^{-2}$. After 512 s of in situ aging, minor changes in peaks originating from vibrational modes from IDIC are observed in the blend spectrum. To demonstrate that the in situ aging results in the formation of the same degradation product, in situ aging of neat IDIC films was also performed, resulting in identical changes to those observed during white LED aging. No changes in the Raman spectrum were observed during in situ aging of PTQ10,

consistent with the lack of changes observed during UV-visible spectroscopy.

To aid with identifying potential photodegradation products, mass spectrometry was performed on samples of IDIC prior to and after 120 h of photoaging, at which point clear changes are visible in both UV-visible and Raman spectra. To minimize fragmentation during characterization, matrix-assisted laser desorption/ionization time-of-flight (MALDI-TOF) mass spectrometry was used. No obvious differences in the spectra could be identified (Figure S5, Supporting Information), demonstrating that potential photodegradation product(s) are mass invariant, and there is no obvious fragmentation occurring.

Due to the lack of any observed mass change and the similar nature of the interunit region between IDIC and ITIC, which has been reported previously to be particularly susceptible to photodegradation within ITIC, the potential photoisomerization degradation pathway reported previously for ITIC was considered as a possible degradation pathway (Figure 6). The product, P1, can undergo further degradation if both ends of the molecule undergo this isomerization, forming P2 (Figure 6). To confirm if these proposed degradation products were being formed as a result of photoexcitation, the Raman spectra of IDIC, P1, and P2 were simulated and compared to the experimental Raman

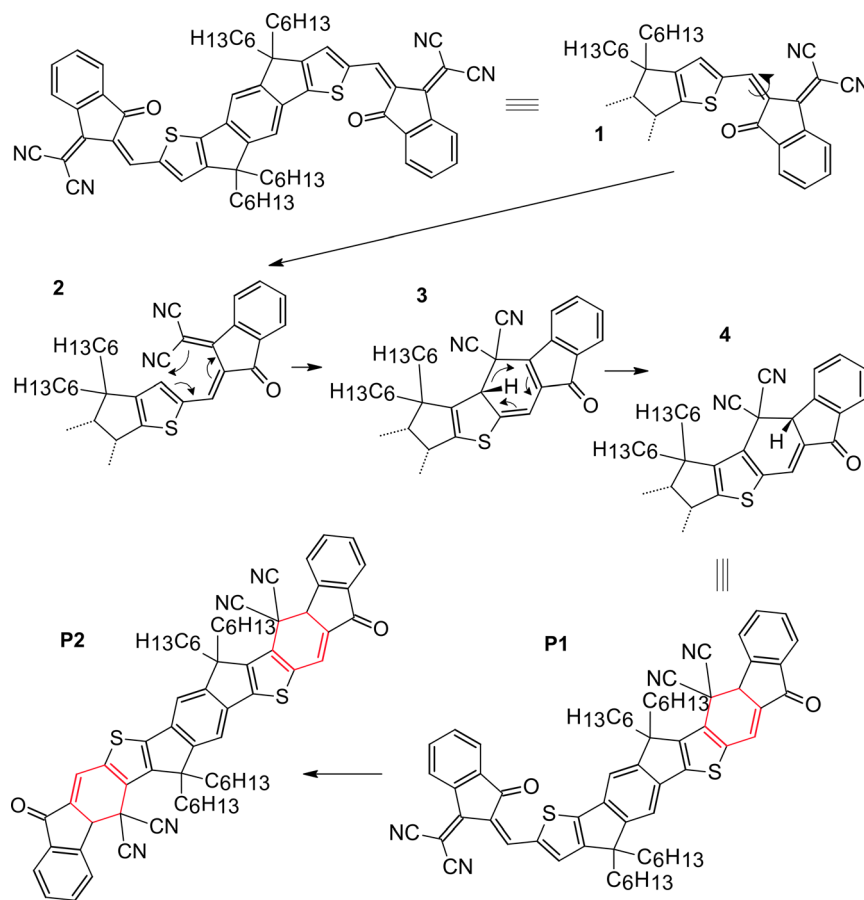


Figure 6. Proposed photodegradation pathway of IDIC, with degradation products P1 and P2. New six-membered rings in P1 and P2 are highlighted in red, based on that proposed for ITIC.^[13]

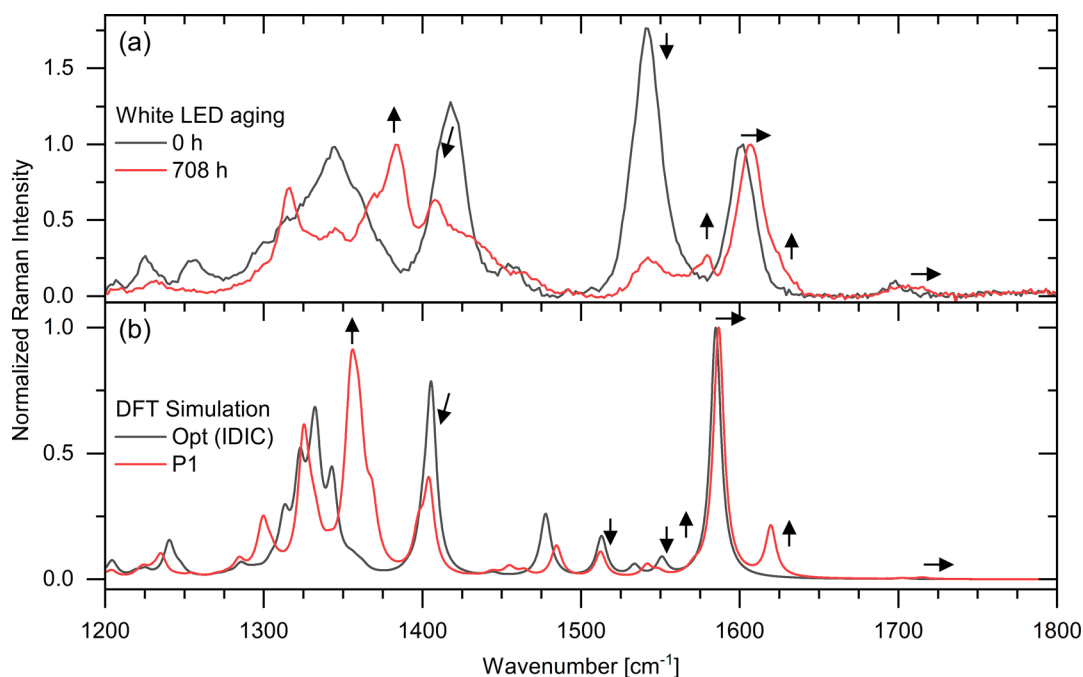


Figure 7. a) Experimentally measured Raman spectra of IDIC prior to and after 708 h of 1 sun equivalent intensity white LED illumination. b) Simulated Raman spectra of IDIC and P1. The arrows correlate with changes discussed in the text.

spectra (Figure 7 and S6, Supporting Information). The spectra are all normalized to the peak at 1600 cm^{-1} (1585 cm^{-1} in simulations). This peak corresponds to the central benzene ring which is unaffected during the considered photodegradation pathway.

Focusing on the changes within the simulation of IDIC to P1 (Figure 7b), there are several peak changes that are also observed in corresponding ITIC simulation.^[29] The peaks associated with the central benzene ring (1585 cm^{-1}) and carbonyl (1715 cm^{-1}) are shifted to higher frequencies. The peak associated with the C=C alkene between the malonitrile and indanone in the end groups of IDIC (1513 cm^{-1}) is strongly quenched. A new low-frequency shoulder emerges at 1572 cm^{-1} , related to the central and terminal benzene rings. The C=C vinylenic alkene peak (1550 cm^{-1}) is also quenched. At 1620 cm^{-1} , a new peak emerges, which is related to the new C=C bond in the alkene within the new six-membered ring.

Additionally, there are further changes that occur exclusively within the IDIC simulation. At 1405 cm^{-1} , the peak associated with the C=C vinylenic and C–C thiophene vibrations simultaneously shifts to lower frequencies and is quenched. There are many overlapping peaks in the lower-frequency region between 1300 and 1375 cm^{-1} that correlate with the C=C end group benzene and C–C interunit vinylenic vibrations, as well as the C–C bonds that directly connect the central benzene to the adjacent thiophenes. Due to the presence of many peaks in this region, analysis here is not trivial. However, a strong peak at 1357 cm^{-1} does grow in this region from IDIC to P1, which is associated with C–C at the base of the thiophene adjacent to the new ring. The changes for P2, where both ends of the molecule are degraded, the changes are similar, but further exacerbated (Figure S6, Supporting Information).

Now comparing the simulated Raman spectra to the experimentally measured Raman spectra, these highlighted changes in the simulations are all observed experimentally. There are however some differences in relative intensity and some small peak shifts and peak broadening, which is attributed to resonant peak enhancements, intermolecular interactions, and increased disorder present in experimentally measured spectra that are not accounted for in the single-molecule gas-phase simulations. The peak changes observed in the experimental spectra that correlate with those observed in simulations are highlighted by the arrows in Figure 7. The experimental spectra are shown alongside the corresponding simulated spectra in Figure S7, Supporting Information. Highlighting a few of the key changes: the peak measured experimentally at 1540 cm^{-1} includes the C=C inter-unit vinylenic, C=C alkene between the malonitrile and indanone groups in the IDIC end groups, and the C–C and C=C bonds on the five-membered carbon rings between the thiophenes and central benzene is strongly quenched after extended illumination. This is in agreement with the quenching of the associated 1513 and 1550 cm^{-1} alkene modes in the simulations. Additionally, the new alkene mode that appears at 1620 cm^{-1} in simulations, associated with the C=C bond in the new six-membered ring, appears experimentally as a high-frequency shoulder on the 1607 cm^{-1} central benzene mode in the aged experimental IDIC spectrum. The overlapping nature of these peaks when measured experimentally may also contribute to the increase in the absolute intensity of the 1607 cm^{-1} peak (Figure 5), alongside the contribution of the increased Raman resonance of the degradation product. At 1580 cm^{-1} , the emergence of a new peak is observed in the simulations as new low-frequency shoulder at 1572 cm^{-1} , related to the central and terminal benzene rings. The strong growth of the peak at

1375 cm^{-1} experimentally, associated with the 1357 cm^{-1} peak in the simulations, is linked to the C–C at the base of the thiophene adjacent to the newly formed ring.

The excellent agreement of the simulation and experimental Raman spectra strongly supports that IDIC suffers from light-induced isomeric change of the interunit region(s). Combined with a lack of experimentally observed mass change after prolonged illumination (Figure S5, Supporting Information), the identical chemical nature of the interunit region to ITIC, and remarkably similar changes in the UV–visible spectrum as are observed for ITIC, IDIC is believed to suffer from the photoisomerization reaction reported previously for ITIC.

The simulated highest occupied molecular orbital (HOMO) and lowest unoccupied molecular orbital (LUMO) levels of IDIC, P1, and P2, also show that this photoisomerization pathway results in a shallower LUMO and larger bandgap (Table 1). This is what is observed experimentally in the UV–visible spectra (Figure 4). These changes in energetics will result in increased energetic disorder and thereby can explain the increased charge trapping that was observed for devices aged under 1 sun equivalent intensity illumination (Figure 3).

To consider why no photodegradation is observed in devices during 1000 lux illumination, the total energy dose is considered. For measurements with 1 sun equivalent intensity white LED photodegradation, with the J_{SC} was matched to that extracted from EQE spectra for AM1.5 G illumination, the illuminance was measured to be $\approx 160\,000$ lux. In terms of total energy absorbed, the high-intensity illumination is approximately accelerated by 160 times compared to 1000 lux illumination. A total of 1126 h of 1000 lux illumination is therefore approximately equivalent to just 7 h of 1 sun illumination, in which time negligible deterioration in performance is observed (Figure S8, Supporting Information). Under 1 sun illumination, the time to reach 80% of the initial performance (T_{80}) is ≈ 153 h. Assuming the photostability directly correlates with the absorbed energy dose, as has been observed during accelerating aging studies,^[21] under continuous 1000 lux illumination, this device is predicted to have a T_{80} of 1020 days.

Interestingly, throughout these investigations, there was no evidence of PTQ10 being unstable. While not an exhaustive study on the stability of PTQ10, the indications of promising photostability of a reported low cost polymer with a simple synthesis is encouraging.^[22] Furthermore, this study suggests that having outstanding intrinsic material photostability may not be critical for indoor applications, opening up the range of materials that could be considered for the manufacturing of indoor OPVs. This is highly beneficial for commercialization as highly performing materials designed for 1 sun applications, that suffer

from poor photostability, could still be used for indoor applications. A wide pool of materials is also highly beneficial for identifying potential low-cost, processable materials that are compatible with large-area manufacturing methods.

3. Conclusion

The photostability of PTQ10:IDIC devices were investigated under white LED illumination with 1 sun equivalent intensity and 1000 lux illumination. Drastically different photostability behavior was observed, with the high-intensity illumination resulting in a 42% loss in initial PCE after 30 days of illumination. Under 1000 lux illumination, no loss in performance was observed after almost 47 days of continuous illumination. IDIC was identified to have poor photostability, resulting in photoinduced deterioration to its light absorption and likely poorer carrier transport due to increased carrier trapping. No mass-varying degradation product was identified from mass spectrometry, indicating that no fragmentation was occurring due to light absorption. Through Raman spectroscopy, a photoisomerization reaction product, similar to that reported previously for ITIC,^[13] was identified as the most probable degradation product, with excellent agreement between simulated and experimental Raman spectra. This was further supported by simulations of these degradation products showing an increased bandgap compared to IDIC, consistent with the observed changes in UV–visible absorption spectroscopy and increased carrier trapping. This work highlights that materials with poor photostability under 1 sun may still be suitable for use in indoor applications, particularly where lifetime requirements may already be lower than those for outdoor applications.

4. Experimental Section

Device and Film Fabrication: All PTQ10:IDIC devices had the following structure: glass/ITO/ZnO/active layer/MoO₃/Ag/glass. The ZnO solution was formulated by dissolving zinc acetate dihydrate (219.5 mg) in 2-methoxyethanol (2 mL) and ethanolamine (60.4 μ L). This solution was dissolved at 60 °C for at least 1 h before spin-coating on cleaned and oxygen-plasma-treated ITO-coated glass substrates at 4000 rpm for 40 s in an ambient atmosphere. Excess solution was wiped away from the edges of the substrates with an isopropyl-alcohol-soaked cotton bud to enable direct contact to the ITO electrodes. The films were then annealed at 150 °C for 10 min. PTQ10 and IDIC were dissolved at a mass ratio of 1:1.5 and total concentration of 25 mg mL⁻¹ in chloroform at 50 °C. The photoactive layer was deposited by spin-coated in a nitrogen-filled glove box by spin-coating at 3500 rpm for 15 s. The coated films were annealed at 120 °C for 10 min. PTQ10 and IDIC were purchased from 1-Material. And, 10 nm of MoO₃ (99.999%) and 100 nm of Ag (99.999%) were deposited by high-vacuum thermal evaporation through a mask. MoO₃ powder was purchased from Strem. Ag pellets were purchased from Kurt J. Lesker. Devices were encapsulated with a UV-curable epoxy purchased from Solarmer Materials Inc. Identical coating parameters were used for coating of films on glass substrates. All solvents were purchased from Sigma Aldrich. PTQ10 was dissolved in chloroform (15 mg mL⁻¹) and coated at 1300 rpm for 15 s to fabricate neat PTQ10 films. IDIC was dissolved in chloroform (18 mg mL⁻¹) and coated at 3500 rpm for 15 s to fabricate neat IDIC films. All neat films were also annealed at 120 °C for 10 min after coating.

Performance and Stability: The 1 sun performance was characterized by an AAA or ABB xenon arc lamp Newport Solar Simulator. Indoor

Table 1. Calculated HOMO and LUMO levels and corresponding bandgap of IDIC, P1, and P2.

Acceptor	HOMO [eV]	LUMO [eV]	E_g [eV]
IDIC	-5.89	-3.65	2.24
P1	-5.89	-3.51	2.38
P2	-5.87	-3.27	2.60

performance was measured within a matt black box to minimize reflections. A 5 W, 4000 K, 36° Phillips CorePro LED spot GU10 dimmable white LED bulb was used as the light source, located ≈ 72 cm from the device being measured. Illuminance and intensity levels for indoor measurements were measured using an International Light Technologies ITL350 spectrophotometer. For stability measurements, an array of white LEDs was used as the light source (spectrum shown in Figure S2, Supporting Information). Devices were held under open-circuit conditions and a current voltage sweep performed approximately once per hour during stability studies. J_{SC} values were matched approximately to that measured from integrated EQE spectra. Throughout all photoaging studies, devices and films were stored in an environmental chamber that was purged with a continuous flow of dry nitrogen. The environmental temperature was kept below 35 °C, monitored with a thermocouple.

Mass Spectrometry: Neat fresh material was supplied directly from the batch of fresh IDIC. For aged samples, a thin IDIC film was coated by spin-coating and aged under white LED illumination. The aged coated film was then scraped off the substrate used a cleaned razor blade and transferred into a sample vial. Samples vials were purged with nitrogen, sealed, and stored in the dark prior to measurement. Spectra were measured using a Bruker UltrafleXtreme MALDI-TOF mass spectrometer, with a smartbeam-II laser. A scan range of 300–3000 Da was used. This was calibrated using a cesium triiodide solution in *trans*-2-[3-(4-*tert*-Butylphenyl)-2-methyl-2-propenyldiene]malononitrile (DCTB) matrix. Provided samples were solvated in high-performance liquid chromatography grade dichloromethane purchased from Fisher. This was mixed at a sample:matrix ratio of 1:49, using a DCTB matrix (purchased from Santa Cruz Biotechnology). The total concentration was 10 mg mL⁻¹ in dichloromethane. An amount of 0.5–1 μ L of solution was deposited onto the MALDI target plate. This was then dried, allowing for co-crystallization of the mixture. The sample was ablated from the target plate using the smartbeam-II laser, resulting in simultaneous desorption and ionization. Ionized molecules were accelerated into a flight tube, using a typical acceleration energy of 20 kV. Negative ion reflection mode was used for data acquisition. A total of 2000–3000 laser shots were used and the data summed to generate the overall spectrum for each sample.

Raman Spectroscopy: Raman spectra were measured using a Renishaw inVia Raman microscope with a 532 nm excitation laser and 1800 lines mm⁻¹ diffraction grating. Rayleigh scattered light was filtered using holographic notch filters. All Raman measurements were performed on encapsulated devices. For accelerated aging studies, the laser spot size was ≈ 60 μ m, with a laser power of 5 mW, reduced from 100 mW with optical filters. This resulted in an approximate power density of 1.8×10^6 W m⁻².

UV-Visible Spectroscopy: UV-visible spectra were measured from films coated on glass substrates, using a bare glass substrate as the reference. All measurements were performed using a Perkin Elmer Lambda 750 spectrophotometer with integrating sphere attachment.

TPV and TPC Measurements: A high-power white LED was used as the broadband light source for TPV measurements. An OSRAM Opto Semiconductors PL520 515 nm laser with 500 ns pulse length was used as the pulsed light source. A Keysight InfiniiVision DSOX2024A oscilloscope was used to measure the voltage transients. For TPC measurements, the device was connected to a 50 Ω resistor, across which the voltage transient was measured. For TPV measurements, devices were held at open circuit and illuminated with a range of light levels from 0.01 to 1.58 Sun, calibrated by matching the J_{SC} to that extracted from EQE spectra for 1 sun AM1.5 illumination. The device was then illuminated with the pulsed laser, across the range of background illumination levels, and voltage transients from the laser pulses were recorded. A mono-exponential was fitted to calculate the lifetime of the generated carriers.^[32] For TPC measurements, the current transient from the laser pulse at different background illumination levels was calculated by measuring the voltage transient across the 50 Ω resistor and using Ohm's law to calculate the current. The generated charge was calculated by integrating the current transient, and the differential capacitance calculated from the ratio of the laser-pulse-generated charge to the laser pulse voltage change (from TPV). The carrier density was calculated by integrating the differential capacitance with respect to the voltage up to the open-circuit voltage at that

illumination level, and dividing by the device area, electronic charge, and film thickness.^[32]

Density-Functional Theory Simulations: Density-functional theory (DFT) simulations were performed using the Gaussian 16 software on the Imperial College High Performance Computing Service and results were visualized using GaussView 6.0.17.^[33] The optimized ground-state geometry and vibrational frequencies of single, gas-phase molecules were calculated using the DFT method at the B3LYP (hybrid) level of theory with the 6–311 G(d,p) basis set. Calculated frequencies were corrected with an empirical scaling factor of 0.97.^[34]

Supporting Information

Supporting Information is available from the Wiley Online Library or from the author.

Acknowledgements

A.J.C. and W.C.T. would like to acknowledge the Materials and Manufacturing Academy (M2A) funding from the European Social Fund via the Welsh Government and EPSRC project EP/L015099/1, the UKRI funding via Innovate UK project 133701, the EPSRC ATIP funding (EP/T028513/1), and NMSF at Swansea University. E.J.Y. and J.S.K. would like to thank EPSRC ATIP and DTP funding. S.K.T. and M.C. would like to thank ERDF for funding SPARC II. W.C.T. and W.L. would like to acknowledge the Foreign Expert Foundation of China funding (grant no. G2023013014L).

Conflict of Interest

The authors declare no conflict of interest.

Data Availability Statement

The data that support the findings of this study are available from the corresponding author upon reasonable request.

Keywords

IDIC, indoor applications, low light, organic photovoltaics, outdoor applications, photostability, Raman spectroscopy

Received: December 11, 2023

Revised: January 12, 2024

Published online:

- [1] Q. Liu, Y. Jiang, K. Jin, J. Qin, J. Xu, W. Li, J. Xiong, J. Liu, Z. Xiao, K. Sun, S. Yang, X. Zhang, L. Ding, *Sci. Bull.* **2020**, *65*, 272.
- [2] P. Bi, C. An, T. Zhang, Z. Chen, Y. Xu, Y. Cui, J. Wang, J. Li, Y. Wang, J. Ren, X. Hao, S. Zhang, J. Hou, *J. Mater. Chem. A* **2023**, *11*, 983.
- [3] X. Zhou, H. Wu, U. Bothra, X. Chen, G. Lu, H. Zhao, C. Zhao, Q. Luo, G. Lu, K. Zhou, D. Kabra, Z. Ma, W. Ma, *Mater. Horiz.* **2023**, *10*, 566.
- [4] E. M. Speller, A. J. Clarke, J. Luke, H. K. H. Lee, J. R. Durrant, N. Li, T. Wang, H. C. Wong, J.-S. Kim, W. C. Tsoi, Z. Li, *J. Mater. Chem. A* **2019**, *7*, 23361.
- [5] X. Du, T. Heumueller, W. Gruber, A. Classen, T. Unruh, N. Li, C. J. Brabec, *Joule* **2019**, *3*, 215.
- [6] X. Xu, J. Xiao, G. Zhang, L. Wei, X. Jiao, H.-L. Yip, Y. Cao, *Sci. Bull.* **2020**, *65*, 208.

- [7] Y. Li, X. Huang, K. Ding, H. K. M. Sheriff, L. Ye, H. Liu, C.-Z. Li, H. Ade, S. R. Forrest, *Nat. Commun.* **2021**, *12*, 5419.
- [8] P. C. Eklund, A. M. Rao, P. Zhou, Y. Wang, J. M. Holden, *Thin Solid Films* **1995**, *257*, 185.
- [9] N. Wang, X. Tong, Q. Burlingame, J. Yu, S. R. Forrest, *Sol. Energy Mater. Sol. Cells* **2014**, *125*, 170.
- [10] A. Distler, T. Sauermann, H.-J. Egelhaaf, S. Rodman, D. Waller, K.-S. Cheon, M. Lee, D. M. Guldi, *Adv. Energy Mater.* **2014**, *4*, 1300693.
- [11] J. Luke, E. M. Speller, A. Wadsworth, M. F. Wyatt, S. Dimitrov, H. K. H. Lee, Z. Li, W. C. Tsoi, I. McCulloch, D. Bagnis, J. R. Durrant, J.-S. Kim, *Adv. Energy Mater.* **2019**, *9*, 1803755.
- [12] M. J. Newman, E. M. Speller, J. Barbé, J. Luke, M. Li, Z. Li, Z. K. Wang, S. M. Jain, J. S. Kim, H. K. H. Lee, W. C. Tsoi, *Sci. Technol. Adv. Mater.* **2018**, *19*, 194.
- [13] Y. Che, M. R. Niazi, R. Izquierdo, D. F. Perepichka, *Angew. Chem. Int. Ed.* **2021**, *60*, 24833.
- [14] A. J. Clarke, J. Luke, R. Meitzner, J. Wu, Y. Wang, H. K. H. Lee, E. M. Speller, H. Bristow, H. Cha, M. J. Newman, K. Hooper, A. Evans, F. Gao, H. Hoppe, I. McCulloch, U. S. Schubert, T. M. Watson, J. R. Durrant, W. C. Tsoi, J. Kim, Z. Li, *Cell. Rep. Phys. Sci.* **2021**, *2*, 100498.
- [15] S. Park, H. J. Son, *J. Mater. Chem. A* **2019**, *7*, 25830.
- [16] Y. Jiang, L. Sun, F. Jiang, C. Xie, L. Hu, X. Dong, F. Qin, T. Liu, L. Hu, X. Jiang, Y. Zhou, *Mater. Horiz.* **2019**, *6*, 1438.
- [17] M. Ghasemi, H. Hu, Z. Peng, J. J. Rech, I. Angunawela, J. H. Carpenter, S. J. Stuard, A. Wadsworth, I. McCulloch, W. You, H. Ade, *Joule* **2019**, *3*, 1328.
- [18] X. Du, T. Heumueller, W. Gruber, O. Almora, A. Classen, J. Qu, F. He, T. Unruh, N. Li, C. J. Brabec, *Adv. Mater.* **2020**, *32*, 1908305.
- [19] B. Watts, W. J. Belcher, L. Thomsen, H. Ade, P. C. Dastoor, *Macromolecules* **2009**, *42*, 8392.
- [20] N. D. Treat, M. A. Brady, G. Smith, M. F. Toney, E. J. Kramer, C. J. Hawker, M. L. Chabinyc, *Adv. Energy Mater.* **2011**, *1*, 82.
- [21] P. Weitz, V. M. Le Corre, X. Du, K. Forberich, C. Deibel, C. J. Brabec, T. Heumueller, *Adv. Energy Mater.* **2023**, *13*, 2202564.
- [22] C. Sun, F. Pan, H. Bin, J. Zhang, L. Xue, B. Qiu, Z. Wei, Z.-G. Zhang, Y. Li, *Nat. Commun.* **2018**, *9*, 743.
- [23] T. Heumueller, T. M. Burke, W. R. Mateker, I. T. Sachs-Quintana, K. Vandewal, C. J. Brabec, M. D. McGehee, *Adv. Energy Mater.* **2015**, *5*, 1500111.
- [24] H. Cha, J. Wu, A. Wadsworth, J. Nagitta, S. Limbu, S. Pont, Z. Li, J. Searle, M. F. Wyatt, D. Baran, J.-S. Kim, I. McCulloch, J. R. Durrant, *Adv. Mater.* **2017**, *29*, 1701156.
- [25] A. Pockett, H. K. H. Lee, B. L. Coles, W. C. Tsoi, M. J. Carnie, *Nanoscale* **2019**, *11*, 10872.
- [26] J. Wu, J. Luke, H. K. H. Lee, P. S. Tuladhar, H. Cha, S.-Y. Jang, W. C. Tsoi, M. Heeney, H. Kang, K. Lee, T. Kirchartz, J.-S. Kim, J. R. Durrant, *Nat. Commun.* **2019**, *10*, 5159.
- [27] J. Wu, J. Lee, Y.-C. Chin, H. Yao, H. Cha, J. Luke, J. Hou, J.-S. Kim, J. R. Durrant, *Energy Environ. Sci.* **2020**, *13*, 2422.
- [28] J. Wu, H. Cha, T. Du, Y. Dong, W. Xu, C. T. Lin, J. R. Durrant, *Adv. Mater.* **2022**, *34*, 2101833.
- [29] J. Luke, E. J. Yang, Y. Chin, Y. Che, L. Winkler, D. Whatling, C. Labanti, S. Y. Park, J. Kim, *Adv. Energy Mater.* **2022**, *12*, 2201267.
- [30] S. Chambon, A. Rivaton, J.-L. Gardette, M. Firon, *Sol. Energy Mater. Sol. Cells* **2007**, *91*, 394.
- [31] S. Chambon, A. Rivaton, J.-L. Gardette, M. Firon, *Sol. Energy Mater. Sol. Cells* **2008**, *92*, 785.
- [32] C. G. Shuttle, B. O'Regan, A. M. Ballantyne, J. Nelson, D. D. C. Bradley, J. de Mello, J. R. Durrant, *Appl. Phys. Lett.* **2008**, *92*, 093311.
- [33] M. J. Frisch, G. W. Trucks, H. B. Schlegel, G. E. Scuseria, M. A. Robb, J. R. Cheeseman, G. Scalmani, V. Barone, G. A. Petersson, H. Nakatsuji, X. Li, M. Caricato, A. V. Marenich, J. Bloino, B. G. Janesko, R. Gomperts, B. Mennucci, H. P. Hratchian, J. V. Ortiz, A. F. Izmaylov, J. L. Sonnenberg, D. Williams-Young, F. Ding, F. Lipparini, F. Egidi, J. Goings, B. Peng, A. Petrone, T. Henderson, D. Ranasinghe, et al., *Gaussian 16, Revision C.07*, Gaussian, Inc., Wallingford CT **2016**.
- [34] M. L. Laury, M. J. Carlson, A. K. Wilson, *J. Comput. Chem.* **2012**, *33*, 2380.